HHS Public Access

Author manuscript

Biol Psychiatry. Author manuscript; available in PMC 2016 September 15.

Published in final edited form as:

Biol Psychiatry. 2015 September 15; 78(6): 374–385. doi:10.1016/j.biopsych.2014.12.029.

Loss of Microtubule-Associated Protein 2 Immunoreactivity Linked to Dendritic Spine Loss in Schizophrenia

Micah A. Shelton, BA[1,2], **Jason T. Newman, PhD**[1,2], **Hong Gu, MS**[4], **Allan R. Sampson, PhD**[4], **Kenneth N. Fish, PhD**[1,2], **Matthew L MacDonald, PhD**[1,2], **Caitlin E. Moyer, PhD**[1,2], **James V DiBitetto, BA**[1], **Karl-Anton Dorph-Petersen, MD, PhD**[1,5,6], **Peter Penzes, PhD**[7,8], **David A. Lewis, MD**[1,2], and **Robert A. Sweet, MD**[1,2,3,9]

[1]Translational Neuroscience Program, University of Pittsburgh School of Medicine, Pittsburgh, PA

[2]Department of Psychiatry, University of Pittsburgh School of Medicine, Pittsburgh, PA

[3]Department of Neurology, University of Pittsburgh School of Medicine, Pittsburgh, PA

[4]Department of Statistics, University of Pittsburgh School of Medicine, Pittsburgh, PA

[5]Translational Neuropsychiatry Unit, Department of Clinical Medicine, Aarhus University, Aarhus, Denmark

[6]Centre for Stochastic Geometry and Advanced Bioimaging, Aarhus University, Aarhus, Denmark

[7]Department of Physiology, Northwestern University Feinberg School of Medicine, Pittsburgh, PA

[8]Department of Psychiatry and Behavioral Sciences, Northwestern University Feinberg School of Medicine, Pittsburgh, PA

[9]Mental Illness Research, Education, and Clinical Center, VA Pittsburgh Healthcare System, Pittsburgh, PA

Abstract

Background—Microtubule-associated protein 2 (MAP2) is a neuronal protein that plays a role in maintaining dendritic structure through its interaction with microtubules. In schizophrenia (Sz), a number of studies have revealed that MAP2's typically robust immunoreactivity (IR) is significantly reduced across several cortical regions. Previous studies have not explored the relationship between MAP2-IR reduction and lower dendritic spine density, which is frequently reported in schizophrenia nor has MAP2-IR loss been investigated in the primary auditory cortex (Brodmann Area 41), a site of conserved pathology in Sz.

For questions and correspondence please contact: Robert A. Sweet, M.D., Mail: Biomedical Science Tower, Rm W-1645, 3811 O'Hara Street, Pittsburgh, PA 15213-2593, Express Mail: Biomedical Science Tower, Rm W-1645, Lothrop and Terrace Streets, Pittsburgh, PA 15213-2593, Phone: 412-624-0064, Fax: 412-624-9910, sweetra@upmc.edu, Web: http://www.wpic.pitt.edu/research/sweetlab/.

These results were presented, in part, at the Annual Meeting of the Society for Neuroscience, Nov 10, 2013, San Diego, California.

MAS, JTN, HG, KNF, MLM, CEM, JVD, K-AD-P, PP, and RAS have no biomedical financial interests or potential conflicts of interest to disclose.

Methods—Using quantitative spinning disk confocal microscopy in two cohorts of Sz subjects and matched control subjects (Sz, n=20; C, n=20), we measured MAP2-IR as well as dendritic spine density and spine number in deep layer 3 of BA41.

Results—Sz subjects exhibited a significant reduction in MAP2-IR. The reductions in MAP2-IR were not associated with neuron loss, loss of MAP2 protein, clinical confounders, or technical factors. Dendritic spine density and number were also reduced in Sz and correlated with MAP2-IR. Twelve (60%) Sz subjects exhibited MAP2-IR values lower than the lowest values in controls; only in this group were spine density and number significantly reduced.

Conclusions—These findings demonstrate that MAP2-IR loss is closely linked to dendritic spine pathology in Sz. Because MAP2 shares substantial sequence, regulatory, and functional homology with MAP tau, the wealth of knowledge regarding tau biology and the rapidly expanding field of tau therapeutics provide resources for identifying how MAP2 is altered in Sz and possible leads to novel therapeutics.

Keywords

Schizophrenia; microtubule-associated protein 2; dendritic spines; auditory cortex; post-mortem human tissue; confocal microscopy

Introduction

Individuals with schizophrenia (Sz) present with a number of functional deficits in the auditory domain. Patients exhibit impaired performance on pure-tone discrimination tasks, an inability which does not depend on attention and thus implicates the auditory cortex itself (1–3). This functional deficit has consequences for social cognition in individuals with the disorder in that it makes prosody detection more difficult (4, 5). In electrophysiological studies, Sz subjects display reduced amplitude on mismatch negativity (MNN) (1, 6–8), an event-related potential generated in the primary auditory cortex in response to stimuli deviant from preceding stimuli with respect to a particular feature (e.g. pitch, amplitude, duration)(9). Performance on tone discrimination tasks and MMN amplitude are correlated, and impairments on both are linked to severity of positive and negative symptoms (1, 3, 10).

These functional and electrophysiological deficits are paralleled at the cortical level by progressive gray matter volume reduction in the superior temporal gyrus (STG) in Sz subjects and first-degree relatives at high risk (11, 12) and specifically in Heschl's gyrus which contains the primary auditory cortex (Brodmann area 41; BA41) (12–16). Reductions in gray matter are found at(12, 16), or prior to transition to,(13–15) the first psychotic episode indicating initial gray matter loss cannot be attributed to the effects of treatment or illness duration. STG gray matter loss is selective for individuals with Sz in comparison to those diagnosed with bipolar disorder (13–15).

Gray matter volume loss in the auditory cortex in Sz is not explained by underlying reductions in layer 3 pyramidal neuron number (17), and more likely represents reductions in pyramidal neuron somal size and excitatory connections in this cortical region (18, 19). We previously described a decrease in the density of spinophillin-immunoreactive puncta in deep layer 3 of the primary auditory cortex in Sz, representing reductions in pyramidal

neuron spine density paralleling findings of a loss of spines per length of dendrite described in other cortical regions (20–22). Sz is also characterized by a reduction in the extent and complexity of the dendritic arbor in hippocampus and cingulate and frontal cortices (21, 23–25). However, the molecular mechanisms that contribute to these concurrent reductions in dendrites and spines in disease are currently unknown.

Microtubule-associated protein 2 (MAP2) stands at the intersection of these phenomena. MAP2 is the most prevalent isoform of the dendritic MAPs, a family of cytoarchitectural proteins that includes the axonal homolog MAP tau (26, 27). MAP2 is an important regulator of neuritic development and maintenance that acts by binding and nucleating the primary structural component of the dendritic cytoskeleton, microtubule (MT) monomers and subsequently stabilizing and spacing mature MT bundles in the dendrite (26–30). MAP2 plays a similar role in supporting the actin cytoskeleton in spines, binding and nucleating filamentous actin (f-actin) to regulate spine morphology (31). MAP2 is regulated by development and experience-dependent plasticity, with these processes tightly controlling MAP2 function by phosphorylation across its functional domains (27). MAP2 immunoreactivity (MAP2-IR) is markedly reduced in a number of different cortical regions associated with Sz pathology including those regions where reduction of the dendritic arbor has been described (32–36) (e.g. cingulate and frontal cortices, hippocampal formation). However, MAP2 mRNA expression levels are unchanged in the disorder suggesting that Sz pathology impacts MAP2 protein and not its transcript (37).

In the present study, we investigated whether MAP2-IR is diminished in deep layer 3 of the primary auditory cortex of Sz subjects and its potential association with spine reduction, which we have previously observed in this layer (18). To address this question, we used multi-label quantitative fluorescence microscopy to measure the intensity of MAP2-IR, spine density, and spine number in 20 subjects with Sz and matched controls. We found that MAP2-IR was significantly decreased in individuals with Sz, with a subset of 60% of Sz subjects that exhibited MAP2-IR levels below the lowest level observed in controls. MAP2-IR was significantly associated with spine density and spine number, with reductions in spine density and number restricted to the 60% of subjects with Sz with MAP2-IR below normal levels. These findings suggest that MAP2 is functionally compromised by disease pathology with implications for dendritic arbor and dendritic spine structural integrity.

Methods and Materials

Human Subjects and Animals

For this study, we used tissue from two cohorts (Table 1) comprised of subjects diagnosed with schizophrenia or schizoaffective disorder (together referred to as Sz) and controls matched on the basis of sex, and as closely as possible for age, post-mortem interval (PMI), and handedness. We also used a previously described monkey (*Macaca fascicularis*) cohort comprised of four animals chronically administered the antipsychotic haloperidol decanoate and age, sex, and weight matched control animals (Fig. 1 top panels, see also supplemental methods section for a more detailed description of human and non-human primate subjects) (18, 38–40).

Immunohistochemistry

Tissue from each cohort was processed together over a series of immunohistochemical runs. In order to visualize dendritic spines, we used two markers in combination: a polyclonal antibody directed against spinophilin (Millipore AB5669, Billerica, MA), a protein that is highly enriched in spine heads (41, 42), and the f-actin binding mushroom toxin phalloidin (Invitrogen A12380, Carlsbad, CA), which also robustly labels spnes (43). MAP2 was detected through the use of mouse monoclonal IgG antibody SMI- 52 (Covance SMI-52R, Princeton, NJ). (See supplemental methods for additional details).

Image Collection

Matched pairs from each cohort were imaged during the same session by an experimenter (JTN) blinded to diagnostic or antipsychotic exposure group. All images were taken using a confocal microscope equipped with a 60× oil supercorrected objective (equipment details found in the supplement). Tissue thickness was measured at each sampling site and did not differ by diagnostic group ($F_{1,18.5}$=0.05, p=0.83) or cohort ($F_{1,18.5}$=2.35, p=0.14). Image stacks were taken beginning 12.5 μm below the tissue surface closest to the coverglass, stepping up 0.25 μm with each image until the tissue surface was reached. This produced an image stack comprised of 50 individual planes, each 512×512 pixels in size. Exposure times for 488nm and 568 nm excitation wavelengths were set to optimize the spread of the intensity histogram for each cohort, then were kept consistent for all subjects within cohorts.

For quantification of MAP2-IR, a single plane was imaged 2 μm beneath the tissue surface at the same sampling sites where image stacks were captured. Each single plane image was taken with an exposure time of 100 ms which was kept constant across all subjects within both human cohorts. The same imaging parameters were used to image the macaque cohort (Fig. 1 bottom panels).

Image Processing

Images were processed using Slidebook software version 5.027 (Intelligent Imaging Innovations, Inc, Denver, Colorado) with keystrokes automated by Automation Anywhere software (Automation Anywhere, Inc. San Jose, CA). Camera background was subtracted from channels 488 and 568 prior to processing. Single plane MAP2 images were masked using a threshold segmentation defined by the Ridler Calvard (RC) derived value in Slidebook. Underlying gray level values were extracted from the mask objects.

Image stacks were deconvolved using the AutoQuant adaptive blind deconvolution algorithm (MediaCybernetics, Rockville, MD). After deconvolution, edges were sharpened by taking the difference between images convolved at two standard deviations of the Gaussian distribution (σ1=0.7; σ2=2.0) as previously described (44), then subjected to iterative intensity/morphological segmentation (45). Spinophilin-IR and phalloidin puncta with intensity measures above the RC defined minimum threshold derived value in Slidebook were selected and contiguous pixels were defined as a ‘mask object.’ Spinophilin-IR and phalloidin mask objects with volumes between 0.1 and 0.8 μm^3 and 0.04 and 1.5 μm^3, respectively, were selected at each iteration. Due to lower spinophilin-IR intensity in cohort 2, it was necessary to begin with a minimum threshold value at 1/3 the RC defined

value. At each of 100 iterations, the threshold intensity was increased and the mask objects combined with those of the prior iteration.

Calculation of Spine Density and Number

While both spinophilin-IR and phalloidin binding are strongly localized to spines, each has some off-target label (42, 43). Therefore, identification of putative dendritic spines required co-localization of spinophilin-IR and phalloidin label (Fig. 2), operationalized as phalloidin mask objects that overlapped (≥ 1 voxel) with a spinophilin-IR mask object. Spine density (N_v) and number (N) in cohort 1 were calculated as previously described with minor modification (39, 40):

$$N_v := \frac{\bar{t}_{wQ^-}}{h} \cdot \frac{\sum \left(Q_i^- \cdot w_i\right)}{BA \cdot a \cdot \sum \left(P_i \cdot w_i\right)}$$

Where *a* is the area of the counting frames, Q_i^- is the count of dendritic spines within the *i*th block, P_i is the count of the associated points hitting the region of interest in the *i*th block, *h* = disector height (see supplemental methods for additional details), *BA* is the cryostat block advance (50 μm for cohort 1 and 60 μm for cohort 2, $\bar{t}_{wQ^-}$ is the block-and-number-weighted mean section thickness calculated using this formula:

$$\bar{t}_{wQ^-} := \frac{\sum \left(t_j \cdot q_j^- \cdot w_i\right)}{\sum \left(q_j^- \cdot w_i\right)}$$

where t_j is the local section thickness measured centrally in the *j*th sampling frame and q_j^- is the corresponding count of dendritic spines in the *j*th frame. w_i is the block weight—i.e. either 1 or 1/3. The number of spines was estimated as the product of previously determined deep layer 3 volumes in these subjects (17, 39, 40) and the N_v calculated in the above equation, represented here:

$$N := N_v \cdot V_{\text{deep layer3}}$$

Because for cohort 2, sections adjacent to the mapping sections were sampled, calculation of N_v and *N* were as above but omitting the block weighting (46).

Statistical Analyses

The intensity of MAP2-IR was log transformed prior to all analyses. Two univariate analysis of covariance (ANCOVA) statistical models, a primary model and secondary model were used to analyze MAP2-IR, spine density, and spine number from our human diagnostic cohort. The primary model included diagnosis, cohort, and pair nested within cohort as blocking factors and tissue storage time as a covariate. To assess the robustness of results, a secondary model was used with diagnosis, cohort, sex, age, PMI, and tissue storage time as covariates ignoring subject pairings (see supplementary methods section for a more detailed explanation of our statistical models). All statistical tests were two-sided with alpha = 0.05.

Results

MAP2 Immunoreactivity

MAP2-IR was significantly reduced in Sz subjects compared to their matched control pairs (Fig. 3) [primary model: $F_{(1,18)}$=18.32; p=0.001 and secondary model: $F_{(1,33)}$=13.88; p=0.001]. There was a 70.0% reduction in log MAP2-IR in Sz subjects relative to controls based on the primary model. The mean log MAP2-IR (SE) for control and Sz subjects was 3.068 (0.085) for controls and 2.545 (0.092) for Sz subjects. The reduction in MAP2-IR is not a result of a reduction in pyramidal neuron number as measured in cohort 1 (Fig. S1) nor is it a consequence of a reduction in the amount of total MAP2 protein (Fig. S2).

Spine Density and Number

Mean spine density was significantly reduced in Sz subjects compared to matched controls [Fig. 4A; primary model: $F_{(1,18)}$=6.17; p=0.023 and secondary model: $F_{(1,33)}$=8.83; p=0.005]. Mean spine density for control subjects [0.0333 μm^{-3} (0.0018)] and Sz subjects [0.0269 μm^{-3} (0.0020)] revealed a 19.22% reduction in spine density.

The reduction in spine density in Sz subjects was paralleled by an accompanying reduction in mean spine number [Fig. 4B; primary $F_{(1,18)}$=4.13, p=0.057 and secondary $F_{(1,33)}$=4.46, p=0.042]. The mean spine number (reported in billions) for control and Sz subjects were 1.30(0.083) and 1.06(0.009) respectively; a 18.79% reduction in spine number across diagnosis. In the secondary model, the effect of cohort was significant [$F_{(1,33)}$=6.33, p=0.017] but the diagnosis by cohort interaction was not significant.

Association with clinical factors

We examined the effect of a number of clinical factors (e.g. sex, manner of death, diagnostic variation, drug exposure, and substance abuse/dependence at time of death) on pairwise percent difference in MAP2-IR, spine density, and spine number. No significant associations were detected. (Table S1).

Correlation between MAP2-IR and Dendritic Spine Density and Number

There was a significant linear correlation between MAP2-IR and spine density (r^2=0.433, p=0.005) but not between MAP2-IR and spine number (r^2=0.162, p=0.32). However, the optimized Kendall's tau approach indicated that MAP2-IR and spine density were significantly related to each other based on the highest Kendall's tau obtained (τ=0.562, z=3.08, p=0.002), as were MAP2-IR and spine number (τ=0.5295, Z=4.48, p<0.001).

Twelve Sz subjects (60%) exhibited MAP2-IR values below the lowest control value, deemed MAP2-IR Low. MAP2-IR Low subjects had significant reductions, relative to their matched controls, in spine density [Fig. 5C; primary: $F_{(1,10)}$=15.970, p=0.003 and secondary: $F_{(1,17)}$=16.9, p=0.001] and spine number [Fig. 5D; primary: $F_{(1,10)}$=12.06, p=0.006 and secondary: $F_{(1,17)}$=12.01,p=0.003]. MAP2-IR Normal Sz subjects did not differ from their matched controls in either spine density [Fig. 5C; primary: $F_{(1,6)}$=0.040, p=0.851 and secondary: $F_{(1,9)}$=0.060, p=0.817] or spine number [Fig. 5D; primary: $F_{(1,6)}$=0.12,p=0.74 and secondary: $F_{(1,9)}$-=0.15,p=0.708].

Antipsychotic Exposed Monkeys

We found no significant effect of chronic haloperidol exposure on MAP2-IR. [Fig. 6; primary $F_{(1,2.77)}$=0.54 p=0.52 and secondary $F_{(1,5.76)}$=0.15 p=0.71]. We previously reported no significant effect of haloperidol exposure on spine density in this group of animals (18).

Discussion

We hypothesized MAP2-IR is reduced in BA41 of individuals with Sz. Using quantitative fluorescence confocal microscopy, we examined alterations in MAP2-IR intensity in BA41 deep layer 3 and examined the relationship between MAP2-IR and dendritic spine markers within the same region. We found that MAP2-IR intensity was significantly reduced in Sz subjects in comparison to matched control subjects. Dendritic spine density and number were also reduced and were associated with MAP2-IR intensity. Twelve (60%) Sz subjects exhibited MAP2-IR intensity levels lower than the lowest control value. In this subset, deemed MAP2-IR Low, there were significant reductions in spine density and spine number while there were no significant reductions in spine density and number in MAP2-IR Normal subjects. Our findings are the first to show a change in MAP2-IR within the auditory cortex of individuals with Sz, and to relate MAP2-IR to dendritic spine alterations.

MAP2-IR Changes Associated with Schizophrenia

We found a significant reduction in MAP2-IR in BA41 deep layer 3. Although the immunoreactive intensity and subcellular location of MAP2 are sensitive to the effects of increasing PMI (Fig. S3), (47) it is unlikely that our finding can be attributed to the effects of PMI or effects of age, sex, and storage time. Our subject pairs were well matched for these variables, mitigating their influence. Moreover, we saw no significant association of any of the aforementioned variables with MAP2-IR within our statistical models, and no significant interactions between them and diagnosis. Similarly, none of the prior studies of MAP2-IR in Sz found significant effects of age, sex, or PMI (32–36). Neither we, nor Rosoklija et al. (34) found a significant effect of antipsychotic treatment. Finally, we examined whether reduced MAP2-IR results from long term antipsychotic exposure in an animal model, and found no effect on MAP2-IR.

Many previous reports have documented reductions in MAP2-IR in other cortical regions linked to Sz pathology (32–36). The drastic nature of the change in IR lends itself to macroscopic observation, which has allowed some groups to qualitatively assess regional IR. Within their cohort, Arnold et al.(36) found a qualitative loss of MAP2-IR in the subiculum and entorhinal cortex of 83% and 66% of their Sz subjects respectively; similar to our observation of marked MAP2-IR loss in the auditory cortex in 60% of our Sz subjects. Rosoklija et al. (34) reported qualitatively low or absent MAP2-IR in the subiculum of 20% of Sz subjects within their cohort but no overall change in IR in comparison to controls within the other hippocampal subfields. In order to quantify this change, others utilized optical density measurements or area fraction analysis (32, 35). As measured by Jones et al. (32), MAP2-IR area fraction was decreased by 45% in layer 5 of frontal cortex (BA9) and 40% in layer 3 of BA9, 44% in layer 5 of cingulate cortex (BA32), and 32% in layer 3 of

BA32 in Sz subjects compared to controls. Somenarain and Jones (35) found a similar result in BA9 area fraction: a 38% reduction in layer 5 and a 39% reduction in layer 3.

Others (32, 35) investigated the relationship between MAP2-IR reductions and neuron loss finding no differences in cell density in areas that showed a disease-specific reduction in MAP2-IR. Similarly, in a previous report (17), the pyramidal neuron number in the twelve pairs that comprise cohort 1 in the present work was determined to be unchanged in BA41 layer 3 (Fig. S1). Arnold et al. (36) found no neuron loss or accompanying increase in markers of neurodegeneration (e.g. gliosis, neurofibrillary tangles) in subjects with a decrease in MAP2-IR, while Rosoklija et al.(34) found no increase in gliosis as assessed by glial fibrillary acidic protein IR. It is clear from these data that neuron loss does not account for reductions in MAP2-IR. Further, using liquid chromatography-mass spectrometry, we have shown that MAP2-IR loss is not a result of protein loss (Fig. S2).

The large number of positive studies, despite the different regions, antibodies, and approach to quantification, in conjunction with evidence that reduced MAP2-IR does not result from common confounds such as PMI, age, and antipsychotic treatment, together lend confidence to the conclusion that reduced MAP2-IR represents a disease-associated alteration present across cortical regions in a large proportion of subjects with Sz. This interpretation raises important questions: what does the decrease in MAP2-IR indicate in terms of molecular changes to MAP2, and what consequences might MAP2-IR loss have for neuronal function in Sz?

Molecular Changes in MAP2 Leading to MAP2-IR Loss

MAP2, like its axonal homolog MAP tau, is tightly regulated by a strict balance of phosphorylation; extremes in either direction lead to decreased MT binding, nucleation, assembly, and stabilization (27, 48–50). It is important to note, that even at intermediate, endogenous levels of phosphate load, site-specific phosphorylation is more important than total phosphate amount in regulating MAP2-MT interaction (48, 51). MAP2 is comprised of four functional domains tasked with different roles: 1) the n-terminal domain, which binds the RII subunit of cAMP-dependent protein kinase A (PKA); 2) the 1372-amino acid (aa) projection domain found only in high molecular weight isoforms of MAP2 (i.e. MAP2A and MAP2B) that regulates the spacing of MT bundles (28); 3) the regulatory proline rich region, and; 4) the microtubule binding domain (MTBD) responsible for binding to MT's and actin (27). A number of protein kinases and phosphatases interact with sites within each region resulting in diverse functional consequences. To illustrate, PKA incorporates phosphate groups at sites primarily within the nterminal and projection domains, thereby disrupting MAP2-MT binding and MT nucleation (52). Similarly, Cdc2 kinase, which phosphorylates the MTBD, also disrupts MAP2-MT binding and MT nucleation, but additionally disrupts MT stabilization (52). Even within functional domains, site-directed kinases can produce highly specific effects (51). Although MAP2 is a natively unfolded protein, it can adopt complex folded conformations; a process that is sensitive to divalent cation concentration and depends on the C-terminal MTBD (51, 53, 54). While not firmly established, it has been proposed that this process could potentially be a result of the high abundance of proline residues within the 156-amino acids adjacent to the MTBD (27, 29).

Proline has the ability to exist in cis- and transisomers based on phosphorylation state and therefore may underlie MAP2's previously observed ability to fold upon itself (54). Phosphorylation-dependent folding has been previously demonstrated in MAP tau models of disease (55). Thus, the reduction of MAP2-IR in our Sz subjects could indicate disease-associated alterations in MAP2 phosphorylation which, via changes in binding to MT targets or in folding, prevents the antibody from reaching its binding site.

It should be noted that other possibilities exist to explain MAP2-IR loss. Rather than a change in MAP2 protein, the phenomenon could represent a change in the network of proteins that bind MAP2. Outside of its role in the cytoskeleton, MAP2 serves as a receptor for the neurosteroids pregnenolone (PREG) and dehydroepiandrosterone (DHEA), an interaction which impacts dendritic stability, changes MAP2 phosphorylation state, and influences MAP2 immunostaining (56, 57). Recent studies have identified changes in serum levels of both of these neurosteroids in patients with first-episode psychosis and linked this phenomenon to symptom severity (58). MAP2 also serves as an anchoring protein linking PKA to class C Ltype Ca^{2+} channels,(59) a class of voltage gated Ca^{2+} channels that have been linked to Sz by genomic studies (60). Genetic studies have also identified genes in the activity-regulated cytoskeleton-associated (*Arc*) pathway that are associated with schizophrenia (61, 62). *Arc* is locally expressed in the dendritic arbor in response to neuronal activity, and it has been demonstrated both *in vivo* and *in vitro* that upregulation of *Arc* reduces MAP2-IR independent of MAP2 protein loss (63). Dysregulation of NMDA receptor activity also changes the subcellular location of the MT plus end capping protein EB3, causing it to bind MAP2 at the MTBD (64). Disease state could potentially alter any of these partners, increasing their MAP2 binding and thus obscuring the antibody epitope. In support of such an interpretation, Cotter et al.(65) found increased MAP2-IR dendritic length in subiculum and hippocampus of subjects with schizophrenia using an antigen retrieval method that disrupts non-covalent protein binding (and/or MAP2 folding), potentially representing a greater unmasking of MAP2-IR sites in schizophrenia subjects.

Potential Consequences of MAP2-IR Loss for Neuronal Function in Schizophrenia

A primary role of MAP2 is stabilizing mature MT bundles in the dendrite (27–30, 66). Recent evidence has elucidated effects of MTs on dendritic spine morphology, finding that dynamic MTs enter developing and mature dendritic spines in response to synaptic activity (67–69). This entry leads to a transition from immature filopodia to mature mushroom head structure in developing spines (68–69). Similarly, MT entry into spines has been demonstrated to be protective against spine reduction induced by long term depression, a process in which MAP2 participates. The link between spine structural plasticity and MAP2 is further supported by findings that inhibition of MT polymerization leads to a loss of mature spine structure, prevents long-term potentiation, and ultimately, ends in a drastic loss of spines themselves (67–69).

We therefore hypothesized that MAP2-IR reductions would be associated with dendritic spine loss in Sz. Our hypothesis was supported by our finding that the reduction in dendritic spines in Sz subjects was restricted to those with substantial reductions in MAP2-IR. Our finding replicated and extended our prior observation that dendritic spine density is

significantly lower in deep layer 3 of primary auditory cortex in individuals with Sz (18). The current observation was made in a non-overlapping cohort of subjects. Furthermore, by using stereologic methods to provide an estimation of spine number, we also showed that the reported loss in spine density reflects a loss of spines themselves as opposed to an expansion in surrounding tissue volume. This finding parallels Golgi-impregnation studies which have documented a Sz-associated loss of layer 3 spine structures per unit of dendrite length in dorsolateral prefrontal cortex(20, 21) and subiculum (22). In addition, the loss of dendritic spines, in the absence of a change in neuron number, can be seen as congruent with earlier hypotheses of reduced neuropil in schizophrenia(70). Given its role in maintaining cell structure, it is plausible that changes to MAP2 protein may also contribute to reduced somal volume, another cellular change previously described in this area of cortex (19).

Summary

We found that 60% of subjects with Sz had dramatic reductions in MAP2-IR in BA41, and that this deficit was correlated with reduced dendritic spine density. The loss of MAP2-IR was not explained by technical factors or subject comorbidities and treatments, suggesting MAP2-IR reduction is a disease-associated alteration. Importantly, reduced MAP2-IR was not due to a loss of MAP2 protein. Future studies will need to identify whether reduced MAP2-IR in Sz results from alterations to MAP2 phosphorylation state, conformation, and/or binding to its interaction partners. This process will be aided by identifying the affected functional domain of MAP2 that contributes to IR reduction, and by investigation of disease-linked changes in the MAP2 protein interactome. Because MAP2 shares substantial sequence, regulatory, and functional homology with MAP tau (26), the wealth of knowledge of tau biology and the rapidly expanding field of tau therapeutics(71) provide resources for identifying how MAP2 is altered in Sz and possible leads to novel therapeutics.

Supplementary Material

Refer to Web version on PubMed Central for supplementary material.

Acknowledgements

This work was supported by National Institutes of Health grants DC011499-03(MAS), MH16804 (MLM), MH096985 (KNF), MH071316 and MH097216 (PP) and MH071533 (RAS).

We thank Dr. C. Sue Johnston for assistance with the clinical data, Mary Brady for design assistance, and the research staff of the Translational Neuroscience Program for technical assistance.

The Biomedical Mass Spectrometry Center and UPCI Cancer Biomarker Facility are supported in part by award P30CA047904.

Financial Disclosures

ARS is a statistical consultant to Janssen Pharmaceutical Research and Development LLC. DAL currently receives investigator-initiated research support from Bristol-Myers Squibb and Pfizer and in 2012-2014 served as a consultant in the areas of target identification and validation and new compound development to Autifony, Bristol-Myers Squibb, Concert Pharmaceuticals, and Sunovion. The content is solely the responsibility of the authors and does not necessarily represent the official views of the National Institute of Mental Health, the National Institutes of Health, the Department of Veterans Affairs, or the United States Government.

References

1. Javitt DC, Shelley A, Ritter W. Associated deficits in mismatch negativity generation and tone matching in schizophrenia. Clin Neurophysiol. 2000; 111:1733–1737. [PubMed: 11018486]
2. Leitman DI, Laukka P, Juslin PN, Saccente E, Butler P, Javitt DC. Getting the cue: sensory contributions to auditory emotion recognition impairments in schizophrenia. Schizophr Bull. 2010; 36:545–556. [PubMed: 18791077]
3. Rabinowicz EF, Silipo G, Goldman R, Javitt DC. Auditory sensory dysfunction in schizophrenia: imprecision or distractibility? Arch Gen Psychiatry. 2000; 57:1149–1155. [PubMed: 11115328]
4. Javitt DC. Sensory processing in schizophrenia: neither simple nor intact. Schizophr Bull. 2009; 35:1059–1064. [PubMed: 19833806]
5. Leitman DI, Ziwich R, Pasternak R, Javitt DC. Theory of Mind (ToM) and counterfactuality deficits in schizophrenia: misperception or misinterpretation? Psychol Med. 2006; 36:1075–1083. [PubMed: 16700967]
6. Naatanen R, Kahkonen S. Central auditory dysfunction in schizophrenia as revealed by the mismatch negativity (MMN) and its magnetic equivalent MMNm: a review. Int J Neuropsychopharmacol. 2009; 12:125–135. [PubMed: 18771603]
7. Umbricht D, Koller R, Schmid L, Skrabo A, Grubel C, Huber T, et al. How specific are deficits in mismatch negativity generation to schizophrenia? Biol Psychiatry. 2003; 53:1120–1131. [PubMed: 12814863]
8. Umbricht D, Krljes S. Mismatch negativity in schizophrenia: a meta-analysis. Schizophr Res. 2005; 76:1–23. [PubMed: 15927795]
9. Javitt DC, Steinschneider M, Schroeder CE, Vaughan HG Jr, Arezzo JC. Detection of stimulus deviance within primate primary auditory cortex: intracortical mechanisms of mismatch negativity (MMN) generation. Brain Res. 1994; 667:192–200. [PubMed: 7697356]
10. Hermens DF, Ward PB, Hodge MA, Kaur M, Naismith SL, Hickie IB. Impaired MMN/P3a complex in first-episode psychosis: cognitive and psychosocial associations. Prog Neuropsychopharmacol Biol Psychiatry. 2010; 34:822–829. [PubMed: 20302901]
11. Mccarley RW, Wible CG, Frumin M, Hirayasu Y, Levitt JJ, Fischer IA, et al. MRI anatomy of schizophrenia. Biol Psychiatry. 1999; 45:1099–1119. [PubMed: 10331102]
12. Rajarethinam R, Sahni S, Rosenberg DR, Keshavan MS. Reduced superior temporal gyrus volume in young offspring of patients with schizophrenia. Am J Psychiatry. 2004; 161:1121–1124. [PubMed: 15169705]
13. Hirayasu Y, Mccarley RW, Salisbury DF, Tanaka S, Kwon JS, Frumin M, et al. Planum temporale and Heschl gyrus volume reduction in schizophrenia: a magnetic resonance imaging study of first-episode patients. Arch Gen Psychiatry. 2000; 57:692–699. [PubMed: 10891040]
14. Kasai K, Shenton ME, Salisbury DF, Hirayasu Y, Onitsuka T, Spencer MH, et al. Progressive decrease of left Heschl gyrus and planum temporale gray matter volume in first-episode schizophrenia: a longitudinal magnetic resonance imaging study. Arch Gen Psychiatry. 2003; 60:766–775. [PubMed: 12912760]
15. Salisbury DF, Kuroki N, Kasai K, Shenton ME, Mccarley RW. Progressive and interrelated functional and structural evidence of post-onset brain reduction in schizophrenia. Arch Gen Psychiatry. 2007; 64:521–529. [PubMed: 17485604]
16. Takahashi T, Wood SJ, Yung AR, Soulsby B, Mcgorry PD, Suzuki M, et al. Progressive gray matter reduction of the superior temporal gyrus during transition to psychosis. Arch Gen Psychiatry. 2009; 66:366–376. [PubMed: 19349306]
17. Dorph-Petersen KA, Delevich KM, Marcsisin MJ, Zhang W, Sampson AR, Gundersen HJ, et al. Pyramidal neuron number in layer 3 of primary auditory cortex of subjects with schizophrenia. Brain Res. 2009; 1285:42–57. [PubMed: 19524554]
18. Sweet RA, Henteleff RA, Zhang W, Sampson AR, Lewis DA. Reduced dendritic spine density in auditory cortex of subjects with schizophrenia. Neuropsychopharmacology. 2009; 34:374–389. [PubMed: 18463626]

19. Sweet RA, Bergen SE, Sun Z, Sampson AR, Pierri JN, Lewis DA. Pyramidal cell size reduction in schizophrenia: evidence for involvement of auditory feedforward circuits. Biol Psychiatry. 2004; 55:1128–1137. [PubMed: 15184031]
20. Garey LJ, Ong WY, Patel TS, Kanani M, Davis A, Mortimer AM, et al. Reduced dendritic spine density on cerebral cortical pyramidal neurons in schizophrenia. J Neurol Neurosurg Psychiatry. 1998; 65:446–453. [PubMed: 9771764]
21. Glantz LA, Lewis DA. Decreased dendritic spine density on prefrontal cortical pyramidal neurons in schizophrenia. Arch Gen Psychiatry. 2000; 57:65–73. [PubMed: 10632234]
22. Rosoklija G, Toomayan G, Ellis SP, Keilp J, Mann JJ, Latov N, et al. Structural abnormalities of subicular dendrites in subjects with schizophrenia and mood disorders: preliminary findings. Arch Gen Psychiatry. 2000; 57:349–356. [PubMed: 10768696]
23. Black JE, Kodish IM, Grossman AW, Klintsova AY, Orlovskaya D, Vostrikov V, et al. Pathology of layer V pyramidal neurons in the prefrontal cortex of patients with schizophrenia. Am J Psychiatry. 2004; 161:742–744. [PubMed: 15056523]
24. Broadbelt K, Byne W, Jones LB. Evidence for a decrease in basilar dendrites of pyramidal cells in schizophrenic medial prefrontal cortex. Schizophr Res. 2002; 58:75–81. [PubMed: 12363393]
25. Kalus P, Muller TJ, Zuschratter W, Senitz D. The dendritic architecture of prefrontal pyramidal neurons in schizophrenic patients. Neuroreport. 2000; 11:3621–3625. [PubMed: 11095531]
26. Dehmelt L, Halpain S. The MAP2/Tau family of microtubule-associated proteins. Genome Biol. 2005; 6:204. [PubMed: 15642108]
27. Sanchez C, Diaz-Nido J, Avila J. Phosphorylation of microtubule-associated protein 2 (MAP2) and its relevance for the regulation of the neuronal cytoskeleton function. Prog Neurobiol. 2000; 61:133–168. [PubMed: 10704996]
28. Belanger D, Farah CA, Nguyen MD, Lauzon M, Cornibert S, Leclerc N. The projection domain of MAP2b regulates microtubule protrusion and process formation in Sf9 cells. J Cell Sci. 2002; 115:1523–1539. [PubMed: 11896199]
29. Farah CA, Leclerc N. HMWMAP2: new perspectives on a pathway to dendritic identity. Cell Motil Cytoskeleton. 2008; 65:515–527. [PubMed: 18473367]
30. Teng J, Takei Y, Harada A, Nakata T, Chen J, Hirokawa N. Synergistic effects of MAP2 and MAP1B knockout in neuronal migration, dendritic outgrowth, and microtubule organization. J Cell Biol. 2001; 155:65–76. [PubMed: 11581286]
31. Selden SC, Pollard TD. Phosphorylation of microtubule-associated proteins regulates their interaction with actin filaments. J Biol Chem. 1983; 258:7064–7071. [PubMed: 6304075]
32. Jones LB, Johnson N, Byne W. Alterations in MAP2 immunocytochemistry in areas 9 and 32 of schizophrenic prefrontal cortex. Psychiatry Res. 2002; 114:137–148. [PubMed: 12113896]
33. Rioux L, Ruscheinsky D, Arnold SE. Microtubule associated protein MAP2 expression in olfactory bulb in schizophrenia. Psychiatry Res. 2004; 128:1–7. [PubMed: 15450909]
34. Rosoklija G, Keilp JG, Toomayan G, Mancevski B, Haroutunian V, Liu D, et al. Altered subicular MAP2 immunoreactivity in schizophrenia. Prilozi. 2005; 26:13–34. [PubMed: 16400226]
35. Somenarain L, Jones LB. A comparative study of MAP2 immunostaining in areas 9 and 17 in schizophrenia and Huntington chorea. J Psychiatr Res. 2010; 44:694–699. [PubMed: 20092829]
36. Arnold SE, Lee VM, Gur RE, Trojanowski JQ. Abnormal expression of two microtubule-associated proteins (MAP2 and MAP5) in specific subfields of the hippocampal formation in schizophrenia. Proc Natl Acad Sci U S A. 1991; 88:10850–10854. [PubMed: 1961755]
37. Law AJ, Weickert CS, Hyde TM, Kleinman JE, Harrison PJ. Reduced spinophilin but not microtubule-associated protein 2 expression in the hippocampal formation in schizophrenia and mood disorders: molecular evidence for a pathology of dendritic spines. Am J Psychiatry. 2004; 161:1848–1855. [PubMed: 15465982]
38. Akil M, Pierri JN, Whitehead RE, Edgar CL, Mohila C, Sampson AR, et al. Lamina-specific alterations in the dopamine innervation of the prefrontal cortex in schizophrenic subjects. Am J Psychiatry. 1999; 156:1580–1589. [PubMed: 10518170]
39. Moyer CE, Delevich KM, Fish KN, Asafu-Adjei JK, Sampson AR, Dorph-Petersen KA, et al. Reduced glutamate decarboxylase 65 protein within primary auditory cortex inhibitory boutons in schizophrenia. Biol Psychiatry. 2012; 72:734–743. [PubMed: 22624794]

40. Moyer CE, Delevich KM, Fish KN, Asafu-Adjei JK, Sampson AR, Dorph-Petersen KA, et al. Intracortical excitatory and thalamocortical boutons are intact in primary auditory cortex in schizophrenia. Schizophr Res. 2013; 149:127–134. [PubMed: 23830684]
41. Allen PB, Ouimet CC, Greengard P. Spinophilin, a novel protein phosphatase 1 binding protein localized to dendritic spines. Proc Natl Acad Sci U S A. 1997; 94:9956–9961. [PubMed: 9275233]
42. Muly EC, Smith Y, Allen P, Greengard P. Subcellular distribution of spinophilin immunolabeling in primate prefrontal cortex: localization to and within dendritic spines. J Comp Neurol. 2004; 469:185–197. [PubMed: 14694533]
43. Capani F, Ellisman MH, Martone ME. Filamentous actin is concentrated in specific subpopulations of neuronal and glial structures in rat central nervous system. Brain Res. 2001; 923:1–11. [PubMed: 11743966]
44. Kirkwood CM, Ciuchta J, Ikonomovic MD, Fish KN, Abrahamson EE, Murray PS, et al. Dendritic spine density, morphology, and fibrillar actin content surrounding amyloid-beta plaques in a mouse model of amyloid-beta deposition. J Neuropathol Exp Neurol. 2013; 72:791–800. [PubMed: 23860033]
45. Fish KN, Sweet RA, Deo AJ, Lewis DA. An automated segmentation methodology for quantifying immunoreactive puncta number and fluorescence intensity in tissue sections. Brain Res. 2008; 1240:62–72. [PubMed: 18793619]
46. Dorph-Petersen KA, Lewis DA. Stereological approaches to identifying neuropathology in psychosis. Biol Psychiatry. 2011; 69:113–126. [PubMed: 20678756]
47. Schwab C, Bondada V, Sparks DL, Cahan LD, Geddes JW. Postmortem changes in the levels and localization of microtubule-associated proteins (tau, MAP2 and MAP1B) in the rat and human hippocampus. Hippocampus. 1994; 4:210–225. [PubMed: 7951696]
48. Brugg B, Matus A. Phosphorylation determines the binding of microtubule-associated protein 2 (MAP2) to microtubules in living cells. J Cell Biol. 1991; 114:735–743. [PubMed: 1907976]
49. Murthy AS, Flavin M. Microtubule assembly using the microtubule-associated protein MAP-2 prepared in defined states of phosphorylation with protein kinase and phosphatase. Eur J Biochem. 1983; 137:37–46. [PubMed: 6140163]
50. Tsuyama S, Bramblett GT, Huang KP, Flavin M. Calcium/phospholipid-dependent kinase recognizes sites in microtubule-associated protein 2 which are phosphorylated in living brain and are not accessible to other kinases. J Biol Chem. 1986; 261:4110–4116. [PubMed: 3949805]
51. Ainsztein AM, Purich DL. Stimulation of tubulin polymerization by MAP-2. Control by protein kinase C-mediated phosphorylation at specific sites in the microtubule-binding region. J Biol Chem. 1994; 269:28465–28471. [PubMed: 7961787]
52. Itoh TJ, Hisanaga S, Hosoi T, Kishimoto T, Hotani H. Phosphorylation states of microtubule-associated protein 2 (MAP2) determine the regulatory role of MAP2 in microtubule dynamics. Biochemistry. 1997; 36:12574–12582. [PubMed: 9376363]
53. Di Noto L, Deture MA, Purich DL. Disulfide-cross-linked tau and MAP2 homodimers readily promote microtubule assembly. Mol Cell Biol Res Commun. 1999; 2:71–76. [PubMed: 10527895]
54. Wille H, Mandelkow EM, Dingus J, Vallee RB, Binder LI, Mandelkow E. Domain structure and antiparallel dimers of microtubule-associated protein 2 (MAP2). J Struct Biol. 1992; 108:49–61. [PubMed: 1373291]
55. Jeganathan S, Hascher A, Chinnathambi S, Biernat J, Mandelkow EM, Mandelkow E. Proline-directed pseudo-phosphorylation at AT8 and PHF1 epitopes induces a compaction of the paperclip folding of Tau and generates a pathological (MC-1) conformation. J Biol Chem. 2008; 283:32066–32076. [PubMed: 18725412]
56. Fontaine-Lenoir V, Chambraud B, Fellous A, David S, Duchossoy Y, Baulieu EE, et al. Microtubule-associated protein 2 (MAP2) is a neurosteroid receptor. Proc Natl Acad Sci U S A. 2006; 103:4711–4716. [PubMed: 16537405]
57. Murakami K, Fellous A, Baulieu EE, Robel P. Pregnenolone binds to microtubule-associated protein 2 and stimulates microtubule assembly. Proc Natl Acad Sci U S A. 2000; 97:3579–3584. [PubMed: 10737804]
58. Ritsner MS. The clinical and therapeutic potentials of dehydroepiandrosterone and pregnenolone in schizophrenia. Neuroscience. 2011; 191:91–100. [PubMed: 21549182]

59. Davare MA, Dong F, Rubin CS, Hell JW. The A-kinase anchor protein MAP2B and cAMP-dependent protein kinase are associated with class C L-type calcium channels in neurons. J Biol Chem. 1999; 274:30280–30287. [PubMed: 10514522]
60. He K, An Z, Wang Q, Li T, Li Z, Chen J, et al. CACNA1C, schizophrenia and major depressive disorder in the Han Chinese population. Br J Psychiatry. 2014; 204:36–39. [PubMed: 24262814]
61. Fromer M, Pocklington AJ, Kavanagh DH, Williams HJ, Dwyer S, Gormley P, et al. De novo mutations in schizophrenia implicate synaptic networks. Nature. 2014; 506:179–184. [PubMed: 24463507]
62. Purcell SM, Moran JL, Fromer M, Ruderfer D, Solovieff N, Roussos P, et al. A polygenic burden of rare disruptive mutations in schizophrenia. Nature. 2014; 506:185–190. [PubMed: 24463508]
63. Fujimoto T, Tanaka H, Kumamaru E, Okamura K, Miki N. Arc interacts with microtubules/microtubule-associated protein 2 and attenuates microtubule-associated protein 2 immunoreactivity in the dendrites. J Neurosci Res. 2004; 76:51–63. [PubMed: 15048929]
64. Kapitein LC, Yau KW, Gouveia SM, Van Der Zwan WA, Wulf PS, Keijzer N, et al. NMDA receptor activation suppresses microtubule growth and spine entry. J Neurosci. 2011; 31:8194–8209. [PubMed: 21632941]
65. Cotter D, Wilson S, Roberts E, Kerwin R, Everall IP. Increased dendritic MAP2 expression in the hippocampus in schizophrenia. Schizophr Res. 2000; 41:313–323. [PubMed: 10708340]
66. Dehmelt L, Halpain S. Actin and microtubules in neurite initiation: are MAPs the missing link? J Neurobiol. 2004; 58:18–33. [PubMed: 14598367]
67. Gu J, Firestein BL, Zheng JQ. Microtubules in dendritic spine development. J Neurosci. 2008; 28:12120–12124. [PubMed: 19005076]
68. Hu X, Viesselmann C, Nam S, Merriam E, Dent EW. Activity-dependent dynamic microtubule invasion of dendritic spines. J Neurosci. 2008; 28:13094–13105. [PubMed: 19052200]
69. Jaworski J, Kapitein LC, Gouveia SM, Dortland BR, Wulf PS, Grigoriev I, et al. Dynamic microtubules regulate dendritic spine morphology and synaptic plasticity. Neuron. 2009; 61:85–100. [PubMed: 19146815]
70. Selemon LD, Goldman-Rakic PS. The reduced neuropil hypothesis: a circuit based model of schizophrenia. Biol Psychiatry. 1999; 45:17–25. [PubMed: 9894571]
71. Wischik CM, Harrington CR, Storey JM. Tau-aggregation inhibitor therapy for Alzheimer's disease. Biochem Pharmacol. 2014; 88:529–539. [PubMed: 24361915]

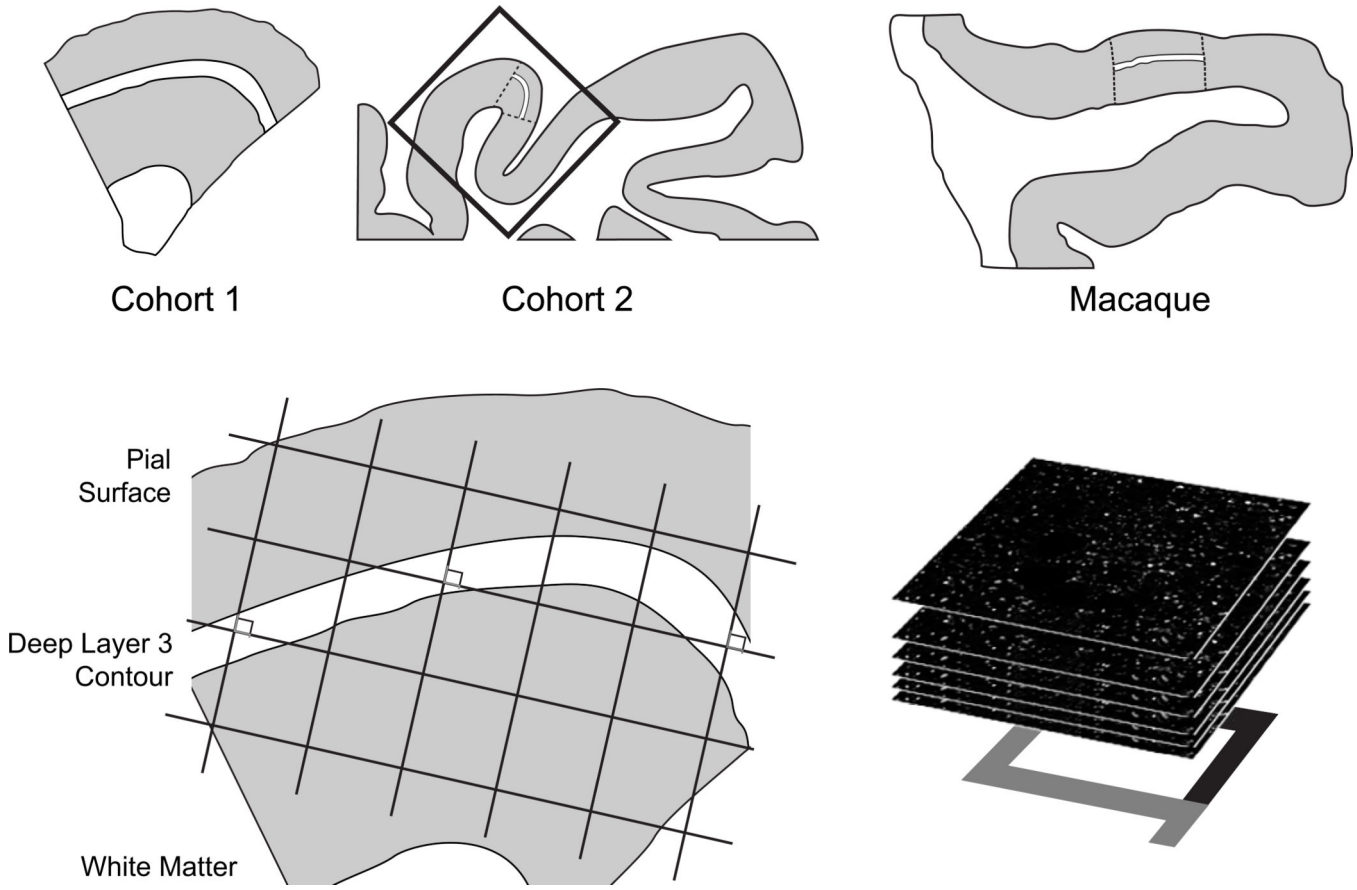

Figure 1. Sampling of primary auditory cortex deep layer 3

(Top) Illustration of delineation of primary auditory cortex deep layer 3 on sections containing auditory cortex for human and antipsychotic exposed macaque cohorts. For each human and monkey subject, the borders of layers 2/3 and 3/4 were identified on adjacent Nissl-stained sections to determine the total layer 3 area for each subject. A contour outline (shown in white) of the deepest one third of layer 3 was drawn in Stereo Investigator (MicroBrightField Inc., Colchester, Vermont). **(Bottom)** A sampling grid was created in Stereo Investigator to generate sampling sites for both human and nonhuman primate subjects. The grid was then randomly rotated, and a sampling site (shown as counting frames) was marked at every intersection between the grid and the deep layer 3 contour. At each sampling site, a 12.5-μm thick stack of 50 image planes, each separated by 0.25 μm, was collected using spinning disk confocal microscopy.

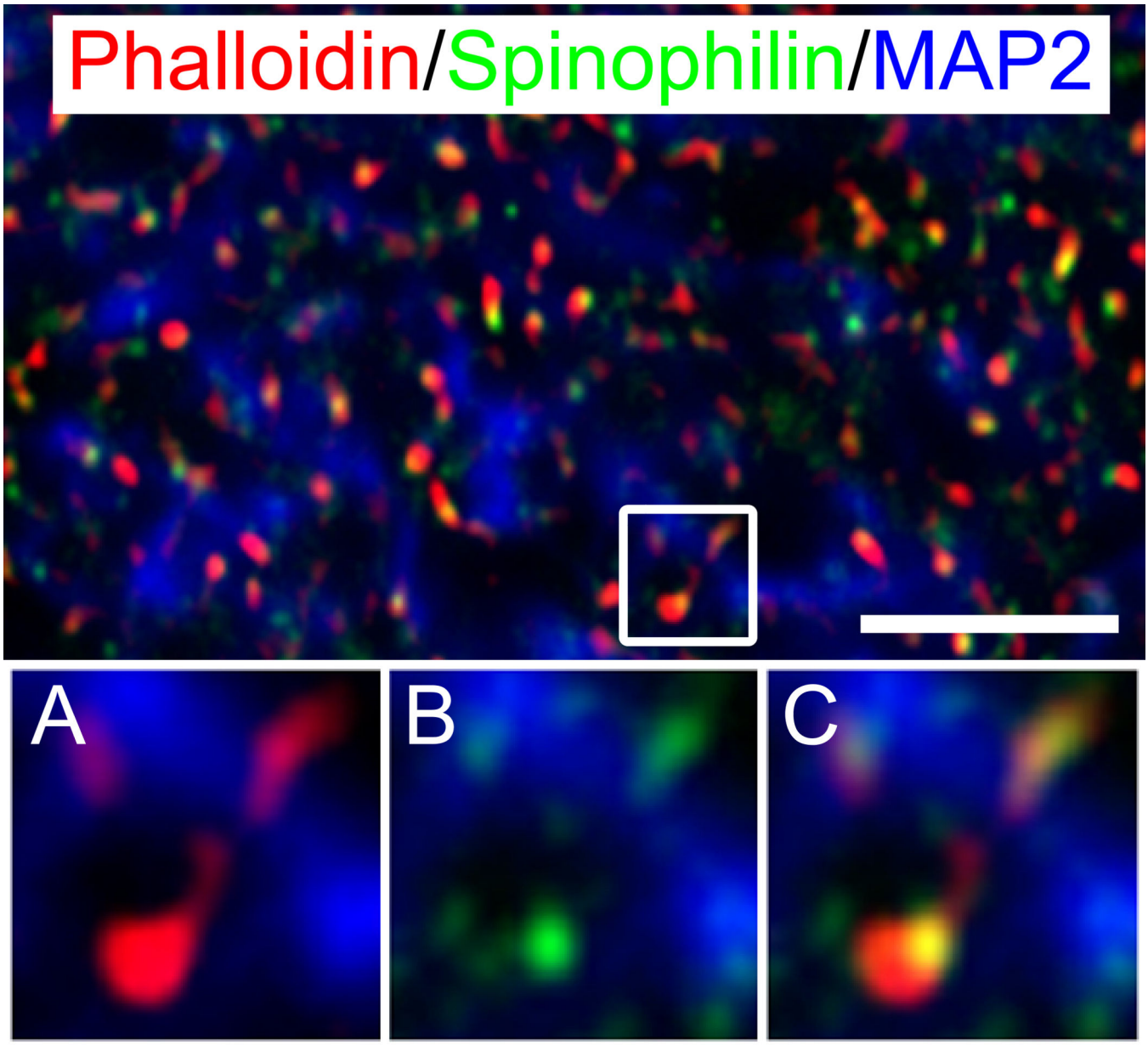

Figure 2. Phalloidin labeled and spinophilin-immunoreactive puncta in deep layer 3 of primary auditory cortex

(Top) Phalloidin labeled puncta (red) and spinophilin-IR puncta (green) co-localize throughout deep layer 3 of Broadmann area 41 and are often organized along microtubule-associated protein 2 (MAP2) immunoreactive processes (blue) suggesting spine structures along dendrites. Images below are a magnification of the inset in the top panel more closely revealing the relationship between phalloidin-labeled (a) and spinophilin-IR objects (b), and their co-localization in putative spine structures (c). Scale bar=5 μm.

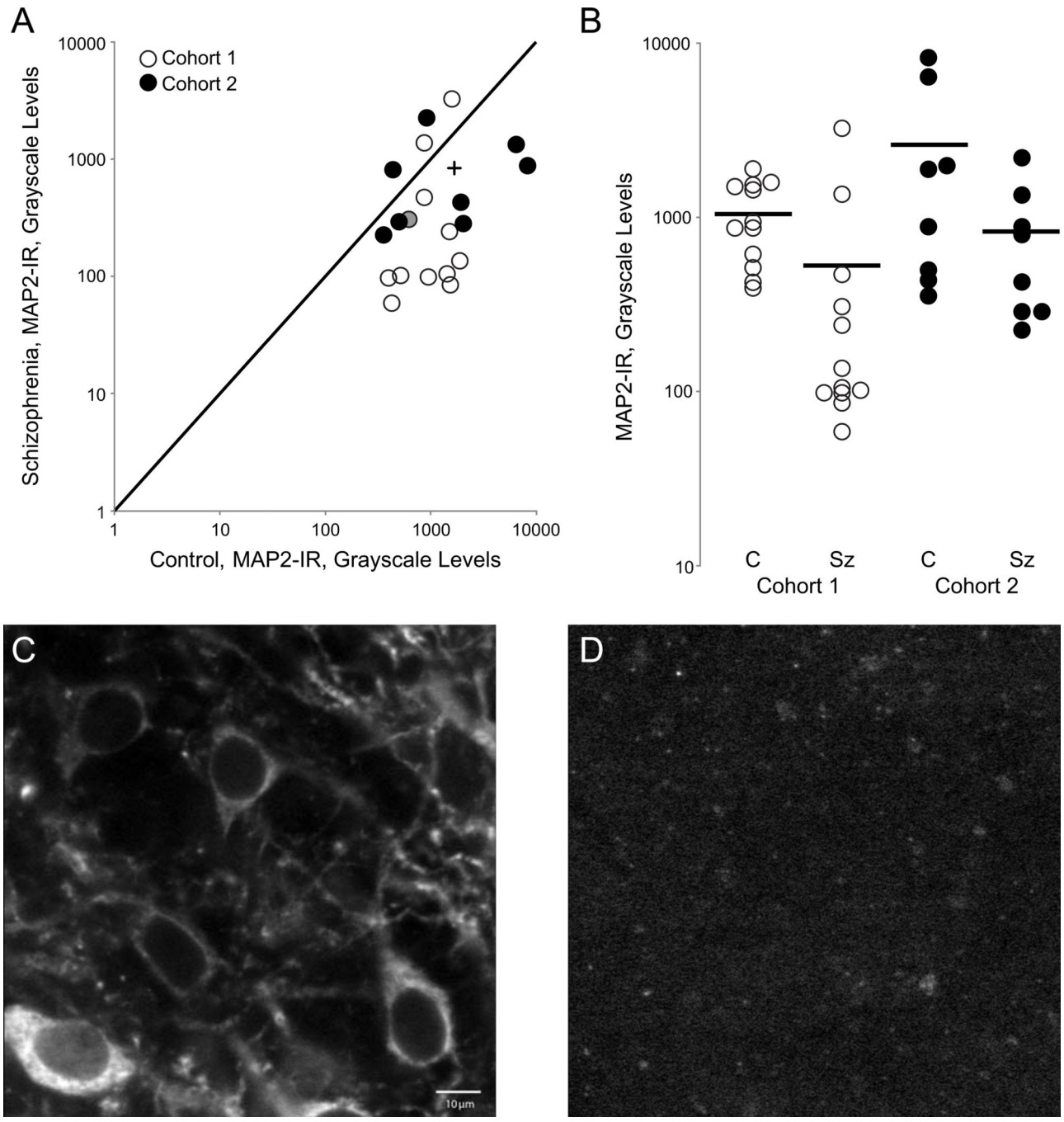

Figure 3. Microtubule-associated protein 2 immunoreactivity (MAP2-IR) is significantly reduced in deep layer 3 of primary auditory cortex in individuals with schizophrenia

(A) MAP2-IR in subject pairs from cohort 1 and cohort 2. The unity line represents schizophrenia=control values; points beneath the line represent pairs in which schizophrenia<control; points above the line represent schizophrenia>control. The plus indicates the group mean. **(B)** MAP2-IR for control (C) and schizophrenia (SZ) subjects in cohort 1 and cohort 2. Bars represent mean IR for each group. (C–D) Representative

micrographs of MAP2-IR taken from a control subject (left) and schizophrenia subject (right); scale bar= 10 μm. (cohort 1, pair 8, filled circle in A).

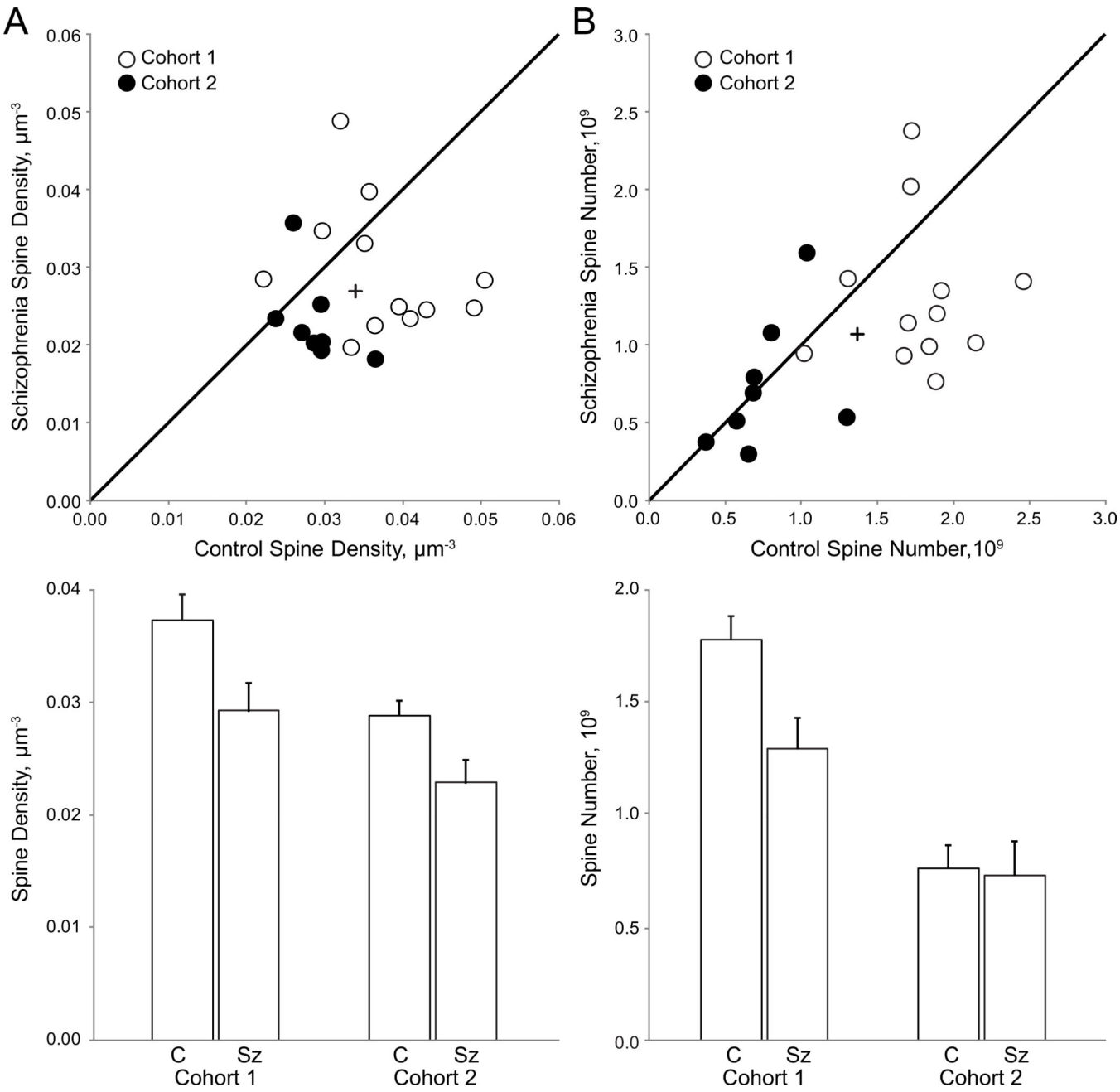

Figure 4. Spine number and density are reduced in deep layer 3 of primary auditory cortex in individuals with schizophrenia

(A) (Top) Mean spine density in deep layer 3 of primary auditory cortex in pairs from cohort 1 and 2. The unity line represents schizophrenia=control values; points beneath the line represent pairs in which schizophrenia<control; points above the line represent schizophrenia>control. The plus indicates the value of the group mean. **(Bottom)** Mean spine density for control (C) and schizophrenia (Sz) subjects in cohort 1 and cohort 2. Error bars are ± SE. **(B) (Top)** Spine number in deep layer 3 of primary auditory cortex in subject pairs. The unity line and plus symbol represent the same relationships as described above.

(Bottom) Mean spine number for control (C) and schizophrenia (Sz) subjects. Error bars are ± SE.

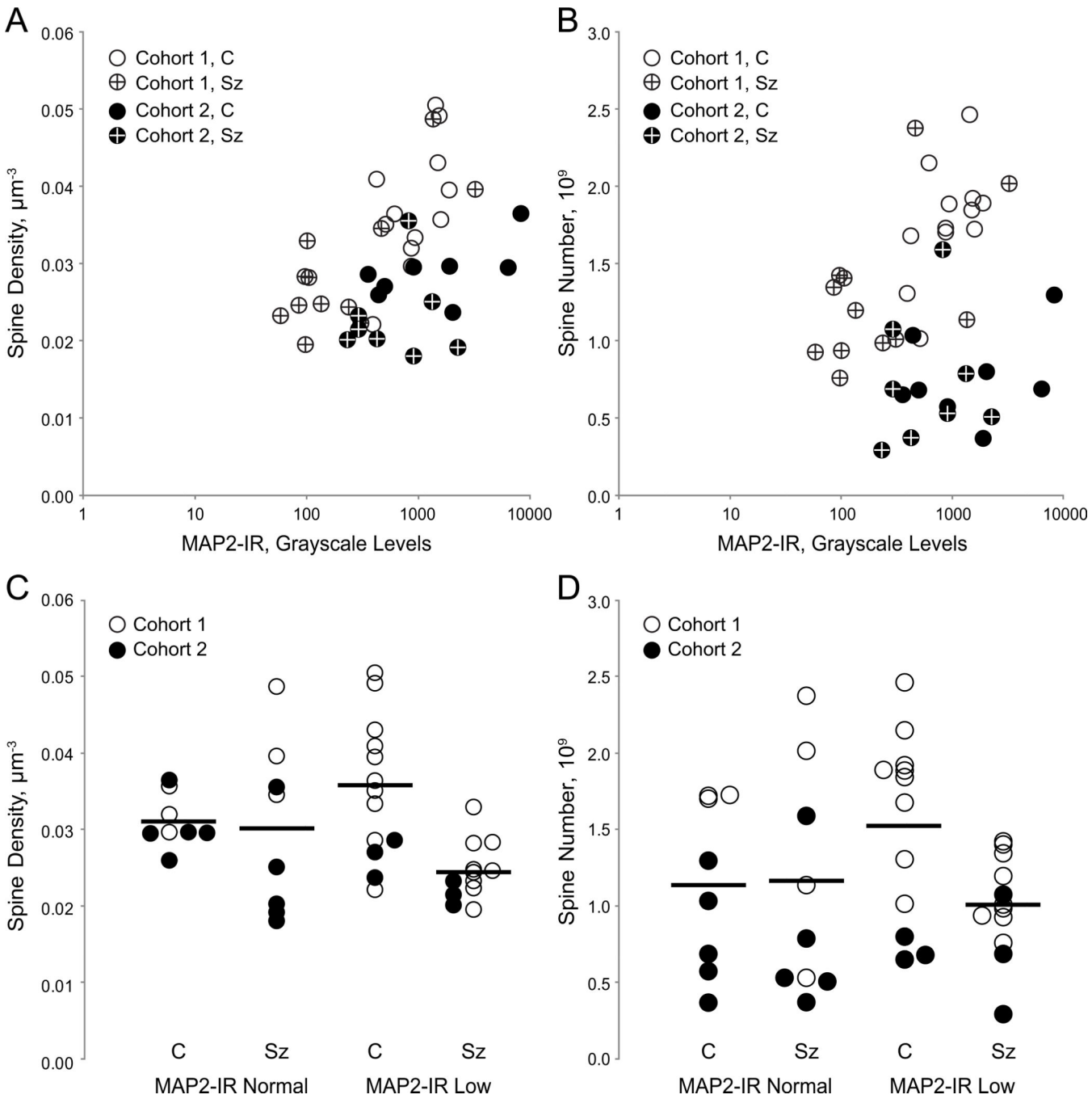

Figure 5. Relationship of microtubule-associated protein 2-immunoreactivty (MAP2-IR) to dendritic spine number and spine density in deep layer 3 of primary auditory cortex

(A) Mean spine density plotted as a function of MAP2-IR for control subjects (open) and schizophrenia subjects (crossed) in cohort 1 (unfilled) and cohort 2 (filled). **(B)** Spine number as a function of MAP2-IR for control subjects (open symbols) and schizophrenia subjects (crossed symbols) in cohort 1 (unfilled) and cohort 2 (filled). **(C)** Spine density for control (C) and schizophrenia (Sz) subjects in pairs in which the Sz subject MAP2-IR was above (MAP2-IR Normal) or below (MAP2-IR Low) the minimum MAP2-IR observed in

control subjects. Bars represent mean values for each group. **(D)** Spine number for control (C) and schizophrenia (Sz) subjects in pairs in which the Sz subject MAP2-IR was above (MAP2-IR Normal) or below (MAP2-IR Low) the minimum MAP2-IR observed in control subjects. Bars represent mean values for each group.

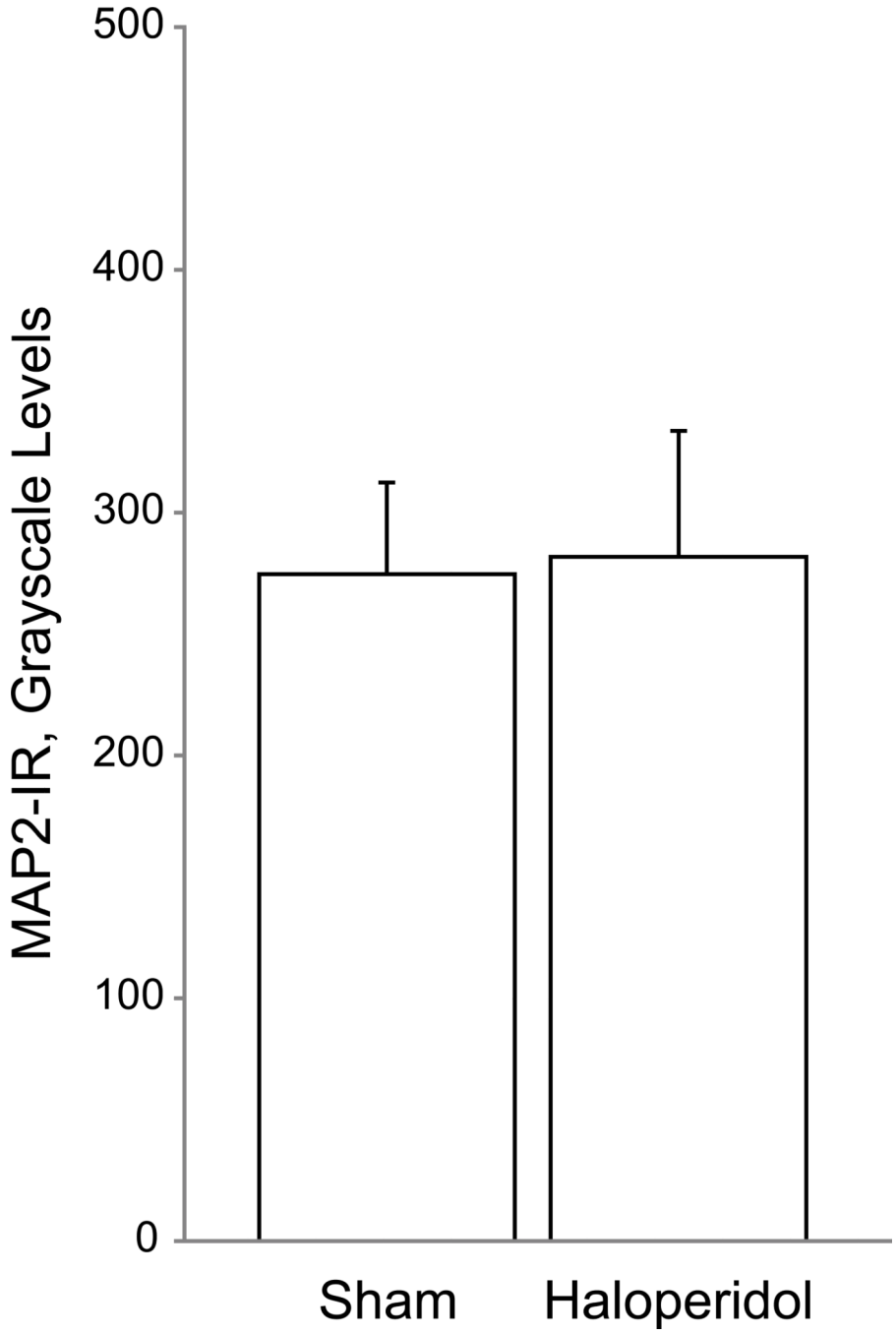

Figure 6. Mean microtubule-associated protein 2 immunoreactivity (MAP2-IR) intensity is unchanged between control and haloperidol-exposed macaques

Chronic antipsychotic exposure did not alter MAP2-IR in adult male macaques. Error bars are ± SEM.

Table 1

Subject Characteristics

Each Sz subject in cohorts 1 and 2 was previously matched to a normal control subject based on sex, and as closely as possible for age and postmortem interval. There were no diagnostic group differences in age [$t(38) = -0.333$, $p = 0.741$] or postmortem interval [$t(38) = -0.272$, $p = 0.787$]. The distribution of handedness between diagnostic groups reached trend level ($\chi 2 = 8.800$, $p = 0.066$). Mean tissue storage time did not differ between diagnostic groups [cohort 1: $t(22) = 0.817$,$p = 0.423$; cohort 2: $t(14) = 0.461$, $p = 0.652$].

	Cohort 1		Cohort 2		Total	
	Control	Sz	Control	Sz	Control	Sz
n	12	12	8	8	20	20
Mean Age, Years (SD)	45.2 (12.9)	47.3 (13.4)	46.4 (14.0)	46.5 (12.4)	45.8 (13.0)	46.9 (13.4)
Range	19–65	27–71	24–62	25–62	19–65	25–71
Sex (F/M)	3/9	3/9	4/4	4/4	7/13	7/13
Handedness (R/L/A/U/)	11/1/0/0	6/2/1/3	8/0/0/0	5/3/0/0	19/1/0/0	11/5/1/3
PMI (SD)	18.1(6.5)	17.9(8.8)	13.7(6.5)	15.6(6.8)	16.4(6.7)	17.0(7.9)
Storage Time, Months (SD)	155.0(27.2)	145.5(29.8)	97.1(22.4)	92.8(14.0)	131.8(38.2)	124.4(35.9)
Illness Duration, Years (SD)		22.1(14.7)		22(13.3)		22.1(13.8)
Range		3–50		4–41		3–50
Age at Onset (SD)		25.2(7.7)		24.5(9.6)		24.9(8.3)
Suicide, n(%)		2(16.7%)		2(25.0%)		4(20.0%)
Schizoaffective, n (%)		4(33.3%)		2(25.0%)		6(30.0%)
Alcohol/ Substance Abuse ATOD		5(41.7%)		0(0%)		5(25.0%)
Anticonvulsant ATOD, n(%)		5(62.5%)		1(12.5%)		6(30.0%)
Antidepressant ATOD, n(%)		3(37.5%)		5(62.5%)		8(40.0%)
Antipsychotic ATOD, n(%)		11(91.7%)		6(75.0%)		17(85.0%)
Benzodiazepine ATOD, n(%)		1(8.3%)		3(37.5%)		4(20.0%)
History of Cannabis Use, n(%)		5(41.7%)		2(25.0%)		7(35.0%)
Tobacco ATOD, n(%)	4(33.3%)	8(66.7%)	3(37.5%)	6(75.0%)	7(35.0%)	14(70.0%)

F, female; M, male; R, right-handed; L, left-handed; A, ambidextrous; U, unknown; PMI, postmortem interval; ATOD, at time of death; SZ, schizophrenia.